INSTITUTE OF PHYSICS PUBLISHING JOURNAL OF PHYSICS B: ATOMIC, MOLECULAR AND OPTICAL PHYSICS

J. Phys. B: At. Mol. Opt. Phys. **36** (2003) 623–636 PII: S0953-4075(03)55243-9

The coherence of qubits based on single Ca^+ ions

F Schmidt-Kaler[1], S Gulde, M Riebe, T Deuschle, A Kreuter, G Lancaster, C Becher, J Eschner, H Häffner and R Blatt

Institut für Experimentalphysik, 6020 Innsbruck, Austria

E-mail: ferdinand.schmidt-kaler@uibk.ac.at

Received 22 October 2002, in final form 13 January 2003
Published 27 January 2003
Online at stacks.iop.org/JPhysB/36/623

Abstract

Two-level ionic systems, where quantum information is encoded in long-lived states (quantum bits, qubits), are discussed extensively for quantum information processing. We present a collection of measurements which characterize the stability of a qubit based on the $S_{1/2}$–$D_{5/2}$ transition of single $^{40}Ca^+$ ions in a linear Paul trap. We find coherence times of $\simeq$1 ms, discuss the main technical limitations and outline possible improvements.

1. Introduction

The concept of quantum computing is based on the coherent manipulation of quantum bits (qubits), which carry the information in a superposition of two quantum mechanical states $\{|0\rangle, |1\rangle\}$ [1–3]. A quantum register is composed out of N qubits. Prior to the computation, the state of all qubits is set to a well defined initial value. During the following computation process, a large number of quantum gate operations is performed on these qubits. This sequence of logic gate operations is determined by the specific task following the desired quantum algorithm. Ideally, during the course of this algorithm the quantum state of the system follows a fully unitary and thus time-reversible path in the 2^N-dimensional Hilbert space, free of any decoherence. Finally, the qubits are projected in the computational basis and the outcome of the algorithm is measured.

However, in contrast to this ideal situation, decoherence will occur and cause errors during the computation process. Thus, highly-entangled quantum states generated during the computation are destroyed and the operation of the quantum computer is affected [4, 5]. Any coupling of the quantum computer to the environment causes decoherence and it seems an impossible task to construct a quantum computer working in an entirely coherent way. Is quantum computing impossible? In order to overcome the problem of decoherence, quantum-error-correction schemes have been proposed [6, 7] which lift the constraint on coherence to an acceptable error rate of about 1 in 10^5 computational steps [2, 8]. Under this condition, error

[1] Author to whom any correspondence should be addressed.

correction schemes show that quantum computation can be performed and will be stabilized against decoherence.

Currently, a number of proposals are being discussed for a future realization of quantum computation, emanating from various fields of physics. We expect that a future quantum computer will fulfil the following list of requirements [3] and any proposal for a future quantum computer should address them. Each system which is proposed for an implementation of a quantum computer will have to provide:

- a scalable physical system with well characterized qubits,
- the ability to initialize the state of the qubits,
- a coherence time much longer than the operation time,
- an universal set of quantum gates: single-qubit and two-qubit gates,
- a qubit-specific measurement.

In this paper we discuss strings of ions for quantum computation [9]: ion strings can be stored in linear Paul traps so that they are arranged in strings, representing a quantum register [1]. They can be optically pumped and optically cooled, such that the register is initialized. Ions are kept under ultra-high vacuum conditions and thus we expect a long coherence time. Initiated by the proposal by Cirac and Zoller [10], other procedures for quantum gate operations have been developed [11] and realized [12]. Single-qubit operations performed by Rabi oscillations have also been shown [13, 14]. For the qubit-specific measurement, the 100% efficient electron shelving technique is employed [15, 16]. Thus, ion-trap quantum is no longer just a theoretical concept in so far as experiments with a small number of qubits have been performed and the properties of the system have been studied in some detail [14, 16, 17].

Here, we focus the discussion to the third item of the above list of requirements: what are the sources of decoherence and how can we investigate them quantitatively? Under the conditions set by the actual experiments [18, 19], we find that the time required for a single logic operation is of the order of 10^1–10^2 μs [20]. Thus, if we demand that the error probability due to decoherence is smaller than 1 in 10^5 we find that a coherence time of at least 1–10 s is required for a successful application of the quantum error correction. In this paper we try to give a deeper insight into the current, mostly technical, limitations of qubit coherence.

Typically with trapped ions, a qubit is encoded in atomic transitions involving levels with extremely low radiative decay: hyperfine ground states are used as qubit bases and manipulated via a far-off resonant Raman transition. An extensive study of the $^9Be^+$ ion for quantum computation is found in [21]. Optionally, the qubit is encoded in a superposition of a ground state $|S\rangle$ and a long-lived metastable state $|D\rangle$ [16, 22], and manipulated on an optical quadrupole transition. For two-qubit gate operations [10, 11], the excitation of motional quantum states [23] in a string of ions [24] is used.

In this paper we consider the qubit transition in $^{40}Ca^+$, from the $S_{1/2}$ ground state to the metastable $D_{5/2}$ state (lifetime $\simeq$ 1 s), and recent experimental investigations of the Innsbruck group [19]. The paper is organized as follows: the first section contains a brief description of the experimental setup and the experimental techniques which are used for trapping, cooling and observing ion strings. In the second section we discuss the coherence of the internal, electronic qubit state $\{|S\rangle, |D\rangle\}$, and in a third section we investigate coherence properties of the lowest motional states $\{|0\rangle, |1\rangle\}$. The final section sketches a proposal of quantum computing using $^{43}Ca^+$ ions, which possibly will allow a large number of quantum logic operations and coherence times that are higher by orders of magnitude than those found for $^{40}Ca^+$ ions.

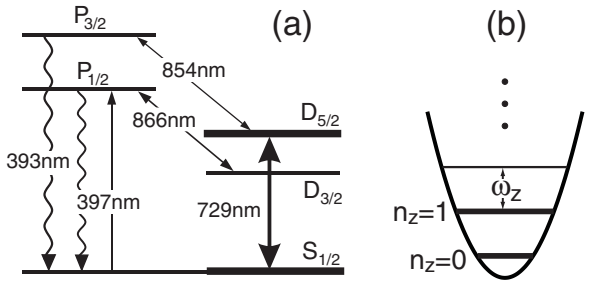

Figure 1. (a) The level scheme of Ca^+ ion. Superpositions of $S_{1/2}$ and $D_{5/2}$ serve as qubits. (b) Vibrational states in the harmonic trapping potential, Fock states $|n = 0\rangle$ and $|n = 1\rangle$ serve as qubits.

2. Experimental setup

For the experiments, a single $^{40}Ca^+$ ion is, or a string of a few ions are, stored in a linear Paul trap. The trapped $^{40}Ca^+$ ion has a single valence electron and no hyperfine structure (see figure 1(a)). We perform Doppler cooling on the $S_{1/2}$–$P_{1/2}$ transition at 397 nm. Diode lasers at 866 and 854 nm prevent optical pumping into the D states. For sideband cooling and for quantum information processing [16], we excite the $S_{1/2}$–$D_{5/2}$ transition with a Ti:sapphire laser near 729 nm (linewidth $\leqslant$ 100 Hz). A constant magnetic field of 2.4 G splits the 10 Zeeman components of the $S_{1/2}$–$D_{5/2}$ multiplet. Depending on the chosen geometry and polarization, the excitation of the $\Delta m = 0, \pm 1$ and ± 2 transitions is allowed. We detect whether a transition to $D_{5/2}$ has occurred by applying the laser beams at 397 and 866 nm and monitoring the fluorescence of the ion on a photomultiplier (electron shelving technique [15]). The internal state of the ion is discriminated with an efficiency close to 100% within 3 ms [16]. The Paul trap is built with four blades separated by 2 mm for radial confinement and two tips separated by 5 mm for axial confinement. Under typical operating conditions we observe for the axial and radial motional frequencies: $(\omega_{ax}, \omega_r)/2\pi = (1.7, 5.0)$ MHz.

2.1. Measurement cycle

The measurement cycle (total duration 20 ms) consists of four consecutive steps:

(I) Doppler cooling (laser 397, 866 and 854 nm on) leads to low thermal vibrational states of axial and radial modes with $\langle n_{ax} \rangle \approx 15$ and $\langle n_r \rangle \approx 3$ phonons.

(II) Sideband cooling of the axial motion is performed on the $S_{1/2}$, $m = -\frac{1}{2}$ to $D_{5/2}$, $m' = -\frac{5}{2}$ transition, leading to a more than 99% ground-state population. Pumping into $S_{1/2}$, $m = +\frac{1}{2}$ is counteracted by several short pulses of σ^- radiation at 397 nm.

(III) Manipulation of the qubit state $|\{S, D\}, \{n = 0, 1\}\rangle$ with radiation near 729 nm.

(IV) Final-state analysis: the ion's fluorescence is collected under excitation with a laser light at 397 and 866 nm and thus the internal state is detected.

This sequence is repeated 100 times so as to measure the $D_{5/2}$ state excitation probability P_D. All experiments, described herein, are performed using this sequence. To investigate different sources for and sorts of decoherence, we just modify step (III) of the sequence according to the specific task.

3. Coherence of the internal qubit state

Qubits are represented by the electronic state $\alpha|\mathrm{S}\rangle + \beta|\mathrm{D}\rangle$ of each ion in the linear string where $|\alpha|^2 + |\beta|^2 = 1$. Decoherence leads to the decay of the quantum mechanical phase relations transforming the above state into an incoherent mixture. Various possible reasons for decoherence on the qubit transition $\mathrm{S}_{1/2}$–$\mathrm{D}_{5/2}$ can be expected:

- qubit energy levels fluctuate via the Zeeman effect caused by ambient magnetic-field fluctuations in the ion trap,
- the laser light driving the qubit transition fluctuates in frequency and light intensity,
- the upper qubit basis state $\mathrm{D}_{5/2}$ decays spontaneously (1 s lifetime).

While the first items are due to technical shortcomings, only the third item is a physical limit for the coherence time. In the following sections, we present a variety of experiments which investigate (and discriminate between) different sources of decoherence as listed above.

3.1. Noise components at 50 Hz

It is well known that electronic devices generate magnetic-field fluctuations at the frequency of 50 Hz (power line). To test the influence of this magnetic-field fluctuations on the qubit levels via the Zeeman shift, we trigger the experimental sequence synchronized to the 50 Hz frequency from the power line. The laser pulse, exciting the qubit transition, always acts at the same instant of time, i.e. when the ion is exposed to about the same ambient magnetic field. The magnitude of the magnetic-field variation at 50 Hz frequency is examined by shifting the excitation pulse in time with respect to the 50 Hz line trigger and measuring the resonance frequency of the $\mathrm{S}_{1/2}(m = -1/2)$–$\mathrm{D}_{5/2}(m' = -5/2)$ with a laser detuning near $\Delta = 0$ ('carrier transition'). The linear Zeeman shift depends on the magnetic g-factors for both states which are involved, $g_{\mathrm{S}_{1/2}} = 2$ and $g_{\mathrm{D}_{5/2}} = 6/5$, and the magnetic quantum numbers m for the initial and final states. Therefore, Zeeman shifts are most sensitively measured via the $m = -1/2 \rightarrow -5/2$ Zeeman component ($\Delta m = 2$) where a field of 1 mG corresponds to a 4.2 kHz shift of the resonance centre.

For this, the laser frequency is varied over the $\mathrm{S}_{1/2}(m = -1/2)$–$\mathrm{D}_{5/2}(m' = -5/2)$ resonance. We record the excitation probability to the upper state, after a 1 ms laser pulse (step (III) of the experimental sequence). The line's central position is determined from a fit to the data. We thus observe, that the centre of the resonance line fluctuates within a bandwidth $\simeq \pm 5$ kHz (figure 2). Even though the details of these fluctuations are not reproduced from day to day, its amplitude remains fairly constant at approximately 1 mG.

To avoid the qubits's dephasing due to the noise (50 Hz), *all* experiments described herein are triggered to the power line frequency. Secondly, to avoid the disturbing influence of the linear Zeeman effect as much as possible, we use the $\mathrm{S}_{1/2}(m = -1/2)$–$\mathrm{D}_{5/2}(m' = -1/2)$ transition ($\Delta m = 0$) for quantum gate operations, with a five times smaller susceptibility for magnetic-field fluctuations.

3.2. Rabi oscillations

The most simple manipulation consists of a single laser pulse in step (III). While the laser detuning $\Delta = 0$ is kept fixed, the pulse length τ is varied. The excitation probability to the $\mathrm{D}_{5/2}$ state is plotted versus the duration τ, and we observe Rabi oscillations as shown in figure 3. In this way single-qubit rotations are realized. From the measured contrast of the oscillations we determine the quality of the qubit rotations. For the given laser intensity here,

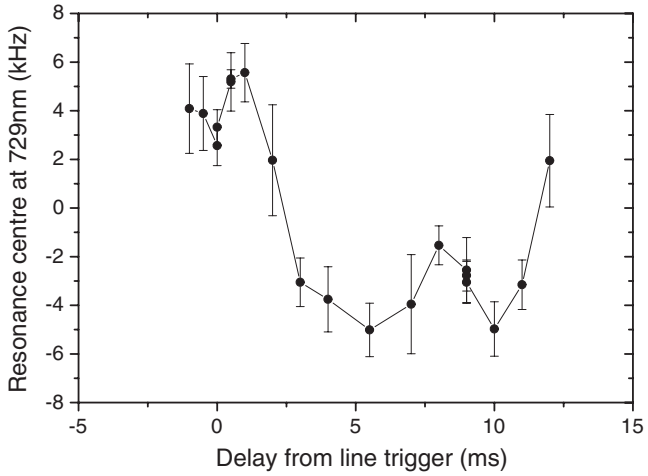

Figure 2. The magnetic-field fluctuations at 50 Hz shift the $S_{1/2}, m = -1/2$ to $D_{5/2}, m = -5/2$ carrier resonance, as the delay between the laser pulse and the line trigger is varied. The interaction time is $\tau = 1$ ms. Note that the vertical bars indicate the width of the observed resonance and not the error of its centre frequency.

a π rotation is achieved after about 7 μs, to implement the logic NOT operation. Even for a 10π rotation we observe a contrast of better than 94% at times near 75 μs. We identify two reasons which limit the contrast:

(i) laser intensity fluctuations cause slightly different Rabi frequencies from shot to shot. As each data point in figure 3 is taken as the average over 100 experimental realizations of the sequence (section 2.1) the contrast is reduced.
(ii) A second limitation of the quality of single-qubit operations is caused by residual small phonon numbers in thermally occupied vibrational modes.

Other than the vibrational mode used for the quantum gate operations, typically not all modes are cooled to the vibrational ground state $|n = 0\rangle$. As the Rabi frequency on the carrier ($\Delta = 0$) transition depends weakly on the phonon occupation number in all those modes ('spectator modes'), averaging over their thermal distributions leads to a reduced contrast [21]. However, this problem can be solved using newly developed cooling techniques [25], which have been demonstrated recently [27]. It can be shown that these cooling techniques will reduce the thermal occupation of all spectator modes of an ion string well below one [26], where their effect on the contrast of Rabi oscillations becomes negligible.

3.3. Ramsey spectroscopy on the $S_{1/2}$ to $D_{5/2}$ transition

Ramsey spectroscopy is perfectly suited for a test of the qubit's decoherence. An initial $\pi/2$ pulse on the carrier ($\Delta \simeq 0$) excites the state $|S\rangle$ and $|D\rangle$ to a coherent superposition. After a second $\pi/2$ pulse, applied after a waiting time, t, the resulting state is projected into the basis $\{|S\rangle, |D\rangle\}$ by the final-state analysis. Varying the laser-frequency detuning Δ yields a Ramsey pattern. Ideally, the excitation $P_D(\Delta)$ to the $D_{5/2}$ state should exhibit a modulation between zero and one when the detuning of the laser frequency is slightly varied.

Experimentally observed Ramsey fringes show $\simeq$99% contrast (figure 4). For the theoretical prediction, two-level-Bloch equations are solved, keeping the length of the $\pi/2$-pulses and the waiting time fixed at the experimental values. Free parameters for the theoretical

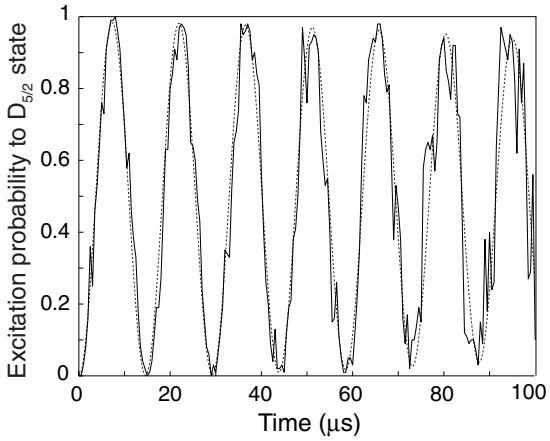

Figure 3. Rabi oscillations on the carrier ($\Delta = 0$) of the $S_{1/2}$ ($m = -1/2$)–$D_{5/2}$ ($m = -1/2$) transition. The numerical simulation (dashed curve) takes into account 3% laser intensity fluctuations and phonon numbers after Doppler and sideband cooling of $n_{rad} = 7, n_{ax} = 0$. From the geometry of the trap and the trap frequencies we calculate the Lamb–Dicke factors for the excitation $\eta_{ax} = 0.068$ and $\eta_{rad} = 0.016$.

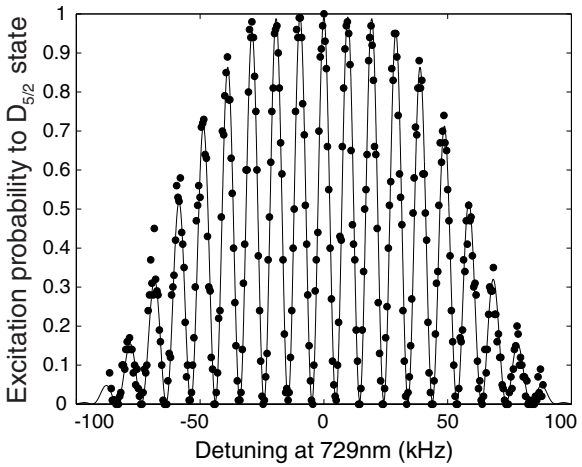

Figure 4. Ramsey spectroscopy on the $S_{1/2}$ ($m = -1/2$)–$D_{5/2}$ ($m = -1/2$) carrier transition ($\Delta \simeq 0$). Each data point is obtained by averaging 100 results of a measurement cycle as described in section 2.1. The scheme consists of a first pulse 9.5 μs in duration followed by a second identical pulse after a waiting time of $t = 100$ μs. For the description of the theoretical curve see the text.

curve are the pulse area of the $\pi/2$-pulses of $\Omega_{\pi/2} = 0.515\pi$ (instead of 0.5π) and the coherence time, accounting for an effective laser linewidth of $\nu_{1/2} = 150$ Hz.

If the superposition of the $|S\rangle$ and the $|D\rangle$ states is exposed to the influence of any decoherence for a long time t, causing a dephasing of the qubit levels, this shows up as a loss of contrast in the observed Ramsey pattern. Systematically we have varied the waiting time t between both the Ramsey pulses from 100 to 1000 μs. The observed contrast $C = (P_D^{max} - P_D^{min})/(P_D^{max} + P_D^{min})$ of the central fringes is plotted versus the waiting time in figure 5. Assuming a white-noise model for the spectral density of the frequency fluctuations, one would expect an exponential $C \sim \exp(-2\pi\nu_{1/2}t)$ to describe the decrease in contrast, and

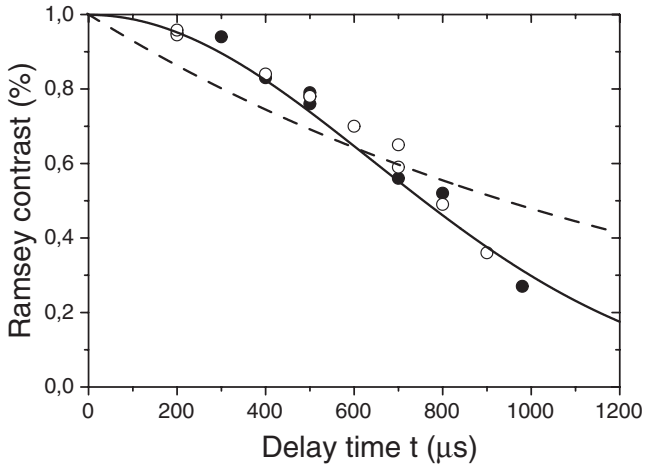

Figure 5. Contrast of the Ramsey pattern as a function of waiting time. Solid (open) circles: data taken without (with) B-field compensation, see text for details. Solid curve: we fit a Gaussian $\sim \exp^{-(t/\tau)^2}$ with $\tau \simeq 0.94(5)$ ms. Dashed curve: optimum exponential fit $\sim \exp^{-t/\tau}$ with the $\tau \simeq 1.4(2)$ ms.

to yield the Lorentzian linewidth $\nu_{1/2}$ [28]. However, the exponential fit to our data is very poor and instead we find that a Gaussian, with a width of $\nu \simeq 170(10)$ Hz, describes our data correctly. Compared to the Lorentzian noise model, the observed noise shows an excess of modulation frequencies $\leqslant$1.5 kHz.

We use an optical fibre to transport the light from the Ti:sapphire laser to the ion-trap setup. This fibre was identified as a source of frequency noise with about 20 Hz [29]. If the fibre-induced noise dominates the frequency noise, we will apply cancellation techniques as described in [31, 32].

To explicitly connect the results shown in figure 5 to the fidelity of the gate operations or to the impurity of the output states of a quantum algorithm [30], we utilize a theoretical model describing the evolution of the density matrix of the whole quantum system as the specific gate operation is performed. In general, the fidelity will decrease as the number of gates and the operation time is increased. However, the description of these numerical simulations is beyond the scope of this paper.

3.4. Active compensation of ambient magnetic-field fluctuations

Since ambient magnetic fluctuations affect the coherence, we have set up an active magnetic-field compensation system [33]. This system consists of a flux gate sensor and a control unit which supplies three orthogonal coils for the cancellation. The specifications of the compensation device claim a bandwidth of 0.5 Hz to 5 kHz. With the aid of an independent flux gate sensor we find that the $\simeq$1 mG ambient field fluctuations (rms) at 50 Hz are reduced by a factor of $\simeq$20.

However, no effect of the cancellation system on the Ramsey contrast is observable as is indicated in figure 5 by the solid circles. As we measure that the bandwidth of the cancellation system is sufficient to suppress noise from 50 Hz to 1 kHz, we assume that the remaining sources of magnetic-field fluctuations are localized in the direct vicinity of the trap and not picked up by the sensor of the cancellation system. In future, we plan to passively shield the trap from any magnetic fluctuations.

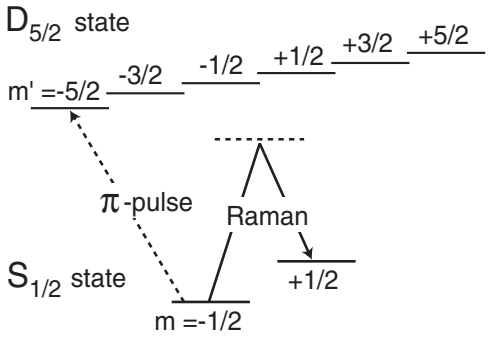

Figure 6. Principle of Raman transitions between Zeeman state $S_{1/2}$, $m = -1/2 \rightarrow m = +1/2$: (i) the ion is prepared in the $m = -1/2$ ground state by optical pumping. (ii) The Raman pulse is applied to excite the $m = +1/2$ ground state. (iii) A π-pulse transfers selectively one of the Zeeman states ($m = -1/2$) to the $D_{5/2}$, $m' = 5/2$ level. After a successful Raman excitation the ion will be detected in the $S_{1/2}$ state, otherwise step (IV) of the experimental sequence (section 2.1) reveals the $D_{5/2}$ state.

3.5. Raman transitions

Further investigations of the magnetic-field fluctuations are performed driving Raman transitions between Zeeman substates $S_{1/2}$, ($m = -1/2$ to $1/2$). For the principle see figure 6.

After preparation steps (I) and (II) in the experimental sequence, in step (III) we drive the Raman transition. Both the laser fields R1 and R2 are generated from the output of the same Ti:sapphire laser by means of an acousto-optical modulator (in double pass configuration), driven with two frequencies. Both beams propagate in the same optical mode, within the same optical fibre [31, 32] and illuminate the ion with a resulting Lamb–Dicke factor of $\eta \simeq 0$. The Raman detuning is $\Delta_R = 500$ kHz. The detuning of R1 is kept fixed, and the frequency of R2 is varied over the resonance. Both light fields are switched on and off together. After this Raman pulse, we use a π pulse on the $S_{1/2}$, $m = -1/2 \rightarrow D_{5/2}$, $m' = -5/2$ for shelving the $m = -1/2$ Zeeman component. Finally, in step IV, the excitation probability of the $D_{5/2}$ state is detected.

The obvious advantage is that the Raman excitation technique is sensitive only to the fluctuations of the ground-state Zeeman levels, but it remains immune to any laser-frequency fluctuations. Its second advantage is a potentially higher susceptibility for magnetic fluctuations, $S_{1/2}$, ($m = -1/2$ to $+1/2$) with 2.8 kHz mG^{-1} and $D_{5/2}$, ($m' = -5/2$ to $+3/2$) with 6.72 kHz mG^{-1} for the transition compared with the $S_{1/2}$ ($m = -1/2$)–$D_{5/2}$ ($m' = -5/2$) resonance of 4.2 kHz mG^{-1}.

We observe Raman spectra and use a 1 ms pulse length for the excitation. The spectra show a linewidth of about 2 kHz. As the width is not given by the Fourier limit according to the pulse duration, we conclude that the fluctuations of the magnetic field are important within 1 ms.

As a result of the dominant 50 Hz component of the ambient magnetic-field fluctuations, the Raman resonance is shifted, depending on the delay time from the 50 Hz trigger pulse (section 3.1). We take various Raman spectra for different delays of the excitation time with respect to the line-trigger, and plot their centre frequencies versus the delay time in figure 7(a). We observe a modulation with the amplitude of a few kiloHertz at a frequency of 50 Hz corresponding to a milliGauss (rms) magnetic-field fluctuation. The active cancellation system reduces this 50 Hz component to about 10% of its initial value, figure 7(b).

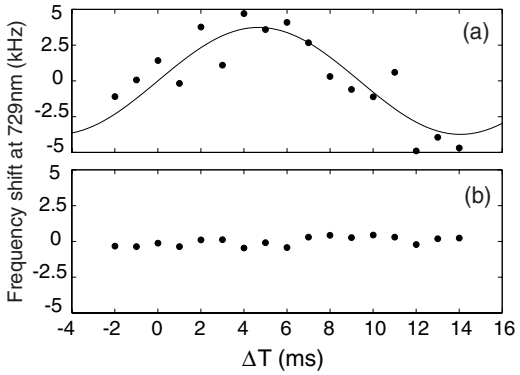

Figure 7. The position of the Raman resonance as a function of laser pulse time delay from the 50 Hz trigger. (a) Without active magnetic-field compensation: we fit a sine function with amplitude 3.8 kHz, corresponding to a 0.75(25) mG field fluctuation. (b) Raman resonance frequency fluctuation using the active compensation, the standard deviation of the data of 0.3 kHz corresponds to magnetic fluctuations of 0.12 mG residual-field fluctuations.

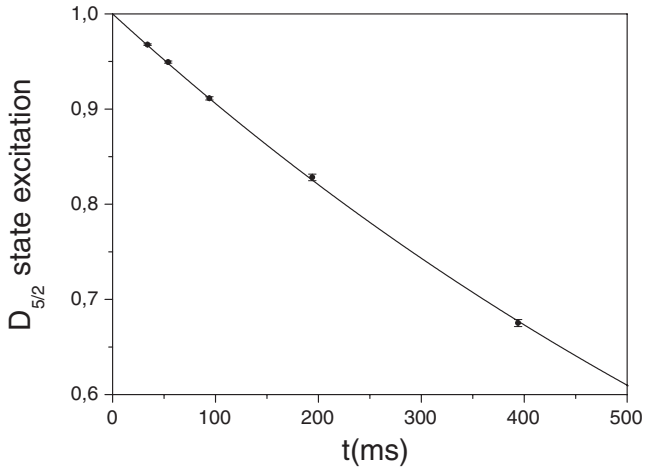

Figure 8. Lifetime measurement of the $D_{5/2}$ state. The collection of data points correspond to a total number of 1.5×10^5 experiments. The errors bars indicate the statistical error. The total data acquisition time was 6.5 h. We find 1011(6) ms (statistical error).

3.6. Lifetime of the $D_{5/2}$ state

The natural lifetime of about $\tau \simeq 1$ s of the $D_{5/2}$ state sets a coherence limit for the single qubit. In order to test the experiment, a single ion is excited to the $D_{5/2}$ state. We record the probability of finding the ion still in the $D_{5/2}$ state after a waiting time t, see figure 8. The resulting value of $\tau = 1011$ ms is slightly below the reported value, see [34] figure 1. With a 6.5 h data acquisition time the statistical error of τ is 6 ms. Systematic errors are discussed in [34, 36]. For example, the $D_{5/2}$ decay may be increased by optical pumping to the ground state via the $P_{3/2}$ state with residual light near 854 nm (see figure 1), explaining the observation of a shorter lifetime [34, 35, 37].

In the experiment, the laser light near 854 nm was switched off using a acousto-optical modulator in double pass configuration with a measured attenuation of $\simeq 2 \times 10^{-4}$. Since

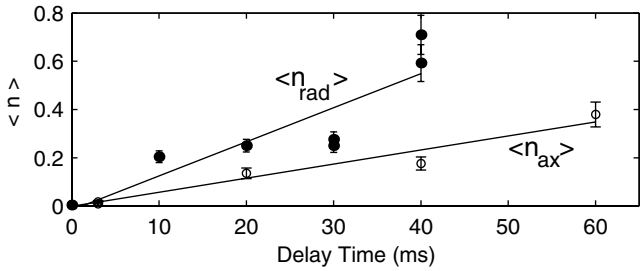

Figure 9. Heating rate measurements for the axial and radial vibrational modes at 4 and 2 MHz, respectively. The heating rates are 1 phonon in 190 ms for the axial and 1 phonon in 70 ms for the radial mode. Construction of the three-dimensional trap was using a ring electrode made of 0.2 mm molybdenum wire with an inner diameter of 1.4 mm (from [16]).

residual light near 854 nm still affects the observed lifetime, we reduced the light power before the acousto-optical modulator for the measurements in figure 8. In addition, the spontaneously emitted broadband background radiation from the diode laser near 866 nm could also have contributed to the reduction in τ [34].

We do not claim to add another value to the literature for the $D_{5/2}$ state lifetime, since this would require a profound investigation into all the systematic errors. However, from the above measurements it is evident that any light that is resonant with the dipole transitions must be suppressed. Note, however, that the coherence of a superposition of the $|S\rangle$ and $|D\rangle$ states would also be affected by an insufficient switching of the laser field near 397 nm. For the light near 397 nm we use two acousto-optical switches and an optical single mode fibre to avoid scattered light (total isolation $\simeq 2 \times 10^{-6}$).

4. Coherence of the motional qubit state

To test the coherence of the motional qubit state, we excite the 'motional qubit', represented by the vibrational states $\{|0\rangle, |1\rangle\}$. For this, the laser-frequency detuning is set to ω_{ax}, the motional sideband frequency, from the S–D resonance.

4.1. Heating rate

If the ion's vibrational state increases without any laser light interaction, we denote this as a heating rate. Systematic studies of heating rates have been performed in a three-dimensional Paul trap [16, 17] and in linear traps [14] for single ions and two-ion crystals. To measure the heating rate, the ion(s) are first cooled to the vibrational ground state. Then the system is left alone for a certain period t to interact with the environment, i.e. with the surrounding electrodes and any possible perturbations acting on the motion of the ions. Finally the resulting vibrational state is analysed.

For all $^{40}Ca^{+}$ ion traps we find that on average it takes about 100 ms to pick up a single phonon. We measure the increasing phonon number by observing the Rabi-flopping signal on the blue sideband. The results of such measurements, the axial phonon numbers $\langle n_{ax}\rangle$ as a function of the delay time t are shown in figure 9. Here, the data obtained for a single ion in the three-dimensional Paul trap, result in a heating rate of $\mathrm{d}\langle n\rangle/\mathrm{d}t = 0.0053\ \mathrm{ms}^{-1}$ (i.e. 1 phonon in 190 ms) at the trap frequency of $\omega_{ax}/(2\pi) = 4$ MHz. For the radial y direction the heating rate is determined to be 1 phonon in 70 ms at $\omega_{rad}/(2\pi) = 1.9$ MHz.

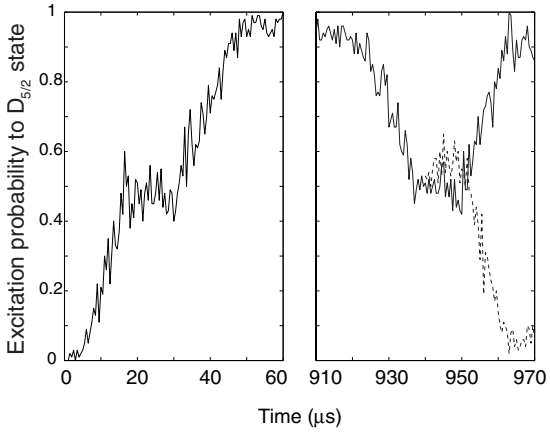

Figure 10. Decoherence of a superposition state of $|n = 0\rangle$ and $|n = 1\rangle$, single ion in the linear trap, for details see text.

While the determination of the heating rate corresponds to the measurement of the T_1 time (denoting energy transfer into the vibrational mode by the coupling to the environment), the following section is dedicated to a measurement of the T_2 time, which quantifies the dephasing of vibrational superposition states [38].

4.2. Decoherence of motional superpositions

To successfully perform two-ion gate operations it is necessary that the motional superpositions do not decohere. In a similar way to the electronic (internal) coherence, we test this with a Ramsey experiment. Thus, we prepare a superposition of two motional states with an identical electronic state. To achieve this we apply a $\pi/2$-pulse on the carrier to obtain $(|n = 0, \mathrm{S}\rangle + |n = 0, \mathrm{D}\rangle)/\sqrt{2}$. Secondly we apply a π-pulse on the blue sideband. This pulse moves the $|n = 0, \mathrm{S}\rangle$-part of the superposition into the $|n = 1, \mathrm{D}\rangle$-state and leaves the $|n = 0, \mathrm{D}\rangle$-part unaffected and we obtain the desired superposition $(|n = 1, \mathrm{D}\rangle + |n = 0, \mathrm{D}\rangle)/\sqrt{2}$). We now wait for a time T before we apply the two laser pulses in the time-reversed order. If no dephasing has occurred during T, this inverse pulse sequence leads to the initial state $|n = 0, \mathrm{S}\rangle$, or $|n = 0, \mathrm{D}\rangle$, depending on the phase of the last laser pulse. Motional decoherence, however, would scramble the phase relation between the $|n = 0, \mathrm{D}\rangle$ and $|n = 1, \mathrm{D}\rangle$ state and thus reduce the contrast.

Figure 10 shows the evolution of the $D_{5/2}$-state population of the excited state P_D as a function of time. For this measurement we repeated the experimental cycle 100 times for each data point, however, we cut off the pulse sequence at the time, t, indicated on the *time* axis. The first pulse is complete at $t = 20$ μs and the second one takes place from $t = 30$ to 60 μs. All laser interactions are interrupted over the interval, T. The pulses are then repeated in reverse order. Depending on the relative phases of the first and the fourth pulse we detect the atom in either the $|\mathrm{D}\rangle$ (solid curve) or the $|\mathrm{S}\rangle$ state (dashed curve). For a waiting time $T = 850$ μs we measure a contrast of 80%, mainly limited by the electronic decoherence which takes place within each pair of pulses. Observing the contrast for various interval times, T, yields a coherence time of approximately 100 ms for the motional superposition state, that is about equal to the motional heating time.

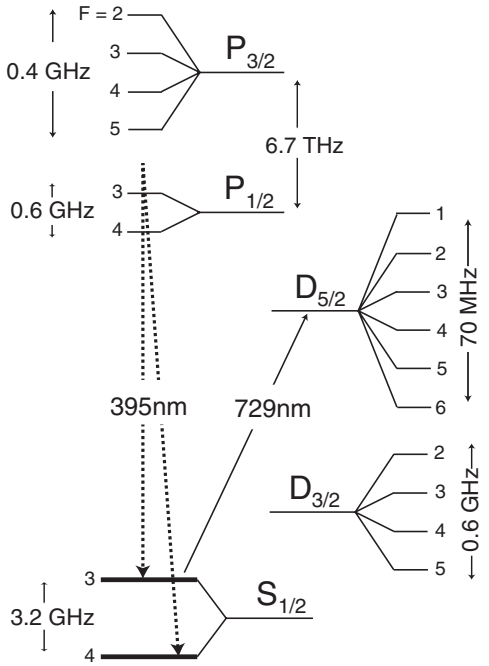

Figure 11. The level scheme of $^{43}Ca^{+}$. Qubit information could be stored in the hyperfine ground states $|S_{1/2}, F = 3, m = 0\rangle$ and $|S_{1/2}, F = 4, m = 0\rangle$. A Raman transition near 396 nm can be used for qubit manipulation. Prior to the state-selective electron shelving, we plan to transfer the $F = 3$ state to the $D_{5/2}$ state with a π-pulse at 729 nm.

5. Future developments

With a systematic investigation of decoherence sources, improvements for a future setup can be devised. We have found for the qubit based on the $S_{1/2}$ to $D_{5/2}$ transition in $^{40}Ca^{+}$ that magnetic-field fluctuations and laser-frequency fluctuations are the major limitations of the present setup. The electronic qubit coherence time is about 1 ms. We measure a coherence time of the motional qubit of about 100 ms.

Major progress is expected to be gained by switching from $^{40}Ca^{+}$ to $^{43}Ca^{+}$, an isotope with nuclear spin $7/2$ which possesses

(i) a hyperfine split ground state and thus long-lived states which may be coupled by Raman transitions, and
(ii) magnetic-field insensitive Zeeman substates which are ideally suited as qubit levels.

Both these properties contribute to potentially much longer coherence times of $^{43}Ca^{+}$, since ambient magnetic fields affect the qubit phase only through the much smaller quadratic Zeeman effect, since spontaneous emission is practically absent, and the laser phase on the Raman transition is controlled by radio-frequency technology and is therefore less susceptible to laser noise.

(iii) By appropriately choosing the directions of the Raman beams with respect to the trap axes, the Lamb–Dicke factor can be optimized such that only the axial, but no radial vibrational modes are excited and thus, radial spectator modes do not affect the gate operation at all.

In addition, the use of Raman transition speeds up quantum gate operations since the two Raman photons transfer a higher recoil to the mode used for the quantum gate [20].

Therefore, we plan to use $^{43}Ca^+$ for quantum computing [39] and to encode the qubit in hyperfine ground states $|S_{1/2}, F = 3, m = 0\rangle$ and $|S_{1/2}, F = 4, m = 0\rangle$. Qubits can be manipulated on the Raman transition, as indicated in figure 6. Doppler cooling may be performed similarly as in $^{40}Ca^+$ on the dipole transitions $S_{1/2}$–$P_{1/2}$. To reach the vibrational ground state, either sideband cooling either on the $S_{1/2}$–$D_{5/2}$ transition, or on the Raman transition between both hyperfine levels can be employed. For the quantum-state detection we will transfer one of the qubit levels, e.g. $|S_{1/2}, F = 3, m = 0\rangle$, to the $D_{5/2}$ state by a resonant carrier π pulse, similar to the scheme presented in figure 6. Eventually, final-state analysis is performed that is similar to the case of $^{40}Ca^+$, i.e. by detecting the fluorescence emitted when the ion is illuminated by resonant radiation near 397 and 866 nm.

With strings of $^{43}Ca^+$ ions we may be able to demonstrate, at the proof-of-concept level, an ion-trap quantum computer using the best features of today's existing experiments thus merging the advantages of experiments on $^{40}Ca^+$ ions with individual addressing and optical qubits, and on $^9Be^+$ ions with the hyperfine encoding of qubits [18].

Acknowledgments

We gratefully acknowledge support by the European Commission (QSTRUCT and QI networks, ERB-FMRX-CT96-0077 and -0087, QUEST network, HPRN-CT-2000-00121, QUBITS network, IST-1999-13021), by the Austrian Science Fund (FWF, SFB15), and by the Institut für Quanteninformation GmbH.

References

[1] Bouwmeester D, Ekert A and Zeilinger A (ed) 2000 *The Physics of Quantum Information* (Berlin: Springer)
[2] Nielsen M A and Chuang I L 2000 *Quantum Computation and Quantum Information* (Cambridge: Cambridge University Press)
[3] DiVincenzo D P 2001 *Quantum. Inf. Comp.* **1** 1
[4] Haroche S and Raimond J M 1996 *Phys. Today* **51**
[5] Mermin N D 2001 *Phys. Today* **11**
[6] Shor P 1995 *Phys. Rev.* A **52** 2493
[7] Steane A 1996 *Phys. Rev. Lett.* **77** 793
[8] Preskill J 1998 *Proc. R. Soc.* A **434** 385
[9] Sarura M and Buzek V 2002 *J. Mod. Opt.* **49** 1593
[10] Cirac I and Zoller P 1995 *Phys. Rev. Lett.* **74** 4714
[11] Sörensen A and Mölmer K 1999 *Phys. Rev. Lett.* **82** 1971
[12] Sackett C A *et al* 2000 *Nature* **404** 256
[13] Nägerl H C *et al* 1999 *Phys. Rev.* A **60** 145
[14] Rohde H *et al* 2001 *J. Opt. B: Quantum Semiclass. Opt.* **3** S34
[15] Nagourney W, Sandberg J and Dehmelt H 1986 *Phys. Rev. Lett.* **56** 2797
Sauter Th, Neuhauser W, Blatt R and Toschek P E 1986 *Phys. Rev. Lett.* **57** 1696
Bergquist J C, Hulet R G, Itano W M and Wineland D J 1986 *Phys. Rev. Lett.* **57** 1699
[16] Roos Ch *et al* 1999 *Phys. Rev. Lett.* **83** 4713
[17] Turchette Q *et al* 2000 *Phys. Rev.* A **61** 063418
[18] http://www.boulder.nist.gov/timefreq/ion/
[19] http://heart-c704.uibk.ac.at/
[20] Steane A *et al* 2000 *Phys. Rev.* A **62** 042305
[21] Wineland D *et al* 1998 *J. Res. Natl Inst. Stand. Technol.* **103** 259
[22] Nägerl H C *et al* 2000 *Phys. Rev.* A **61** 023405
[23] James D F V 1998 *Appl. Phys.* B **66** 181
[24] Nägerl H C, Leibfried D, Schmidt-Kaler F, Eschner J and Blatt R 1998 *Opt. Express* **3** 89

[25] Morigi G, Eschner J and Keitel C H 2000 *Phys. Rev. Lett.* **85** 4458
[26] Schmidt-Kaler F *et al* 2001 *Appl. Phys.* B **73** 807–14
[27] Roos C F *et al* 2000 *Phys. Rev. Lett.* **85** 5547
[28] Sengstock K *et al* 1994 *Appl. Phys.* B **59** 99
[29] Rohde H 2001 *PhD Thesis* Innsbruck, Austria (unpublished)
[30] Gulde S *et al* 2003 *Nature* **421** 48
[31] Ma L S, Junger P, Ye J and Hall J 1994 *Opt. Lett.* **19** 1777
[32] Young B C *et al* 1999 *14th Int. Conf. on Laser Spectroscopy* (Singapore: World Scientific) p 61
[33] FCS-12 Field Cancelling System, Oxford Instruments
[34] Barton P *et al* 2000 *Phys. Rev.* A **62** 032503
[35] Gudjons T, Hilbert B, Seibert P and Werth G 1996 *Europhys. Lett.* **33** 595
[36] Block M, Seibert P, Rehm O and Werth G 1999 *Eur. Phys. J.* D **7** 461
[37] Knoop M, Vedel M and Vedel F 1995 *Phys. Rev.* A **52** 3763
[38] Turchette Q *et al* 2000 *Phys. Rev.* A **62** 053807
[39] Steane A 1997 *Appl. Phys.* B **64** 623